Fracture toughness assessment of a solder joint using double cantilever beam specimens

Lee, Adeline Puay Chen; Lim, Zan Xuan; Yantara, Natalia; Loo, Shane Zhi Yuan; Tee, Tong Yan; Tan, Cher Ming; Chen, Zhong

2008

Lee, A. P. C., Lim, Z. X., Yantara, N., Loo, S. Z. Y., Tee, T. Y., Tan, C. M., et al. (2008). Fracture toughness assessment of a solder joint using double cantilever beam specimens. In proceedings of the 10th Electronics Packaging Technology Conference: Singapore, (pp.1066-1073).

https://hdl.handle.net/10356/91518

https://doi.org/10.1109/EPTC.2008.4763571

Fracture Toughness Assessment of a Solder Joint using Double Cantilever Beam Specimens

Puay Chen Lee Adeline, Zan Xuan Lim[a], Natalia Yantara[a], Shane Loo[a,b], Tong Yan Tee[b],
Cher Ming Tan[c], Zhong Chen[a,]*
[a] School of Materials Science and Engineering, Nanyang Technological University, Singapore 639798
[b] Amkor Technology Singapore Pte Ltd, 2 Science Park Drive, Singapore 118222
[c] School of Electrical and Electronic Engineering, Nanyang Technological University, Singapore 639798
*Tel: (65) 6790 4256; Fax: (65) 6790 9081; Email: aszchen@ntu.edu.sg

Abstract
Conventional assessment of solder joint reliability uses either ball shear test or solder ball pull test. The test results are reported in terms of materials strength in either shear or tensile mode, and the strength values are size-dependent. Therefore these test results are largely useful only for qualitative comparison and qualification of the products. In the current effort, we aim at developing an assessment scheme for solder joint interface fracture toughness. The obtained results, in terms of critical energy release rate, predict the joint failure based on the principle of fracture mechanics. The results can be used as a materials property in the reliability design of various types of solder-ball joined packages. Double cantilever beam (DCB) specimens made of 99.9 wt% copper were selected in the current work. Eutectic Sn-37Pb solder was used to join two pieces of the copper plates with controlled solder thickness. The test record showed steady propagation of the crack along the solder / copper interface, which verifies the viability of such a testing scheme. Interface fracture toughness for as-joined, extensively-reflowed and thermally aged samples has been measured. Both the reflow treatment and the thermal aging lead to degradation of solder joint fracture resistance. To understand the degradation, fractographic analysis by scanning electron microscopy (SEM) has been carried out from both top and cross-sectional views of the fractured surfaces.

1.0 Introduction

The shift from wire bonding to array interconnects such as flip-chip, ball grid arrays and wafer level package technologies is a result of the miniaturization trend to reduce the footprint of electronic chips. As the size gets smaller, solder joint reliability emerged as one of the leading critical issues as it concerns the interconnection of devices on the board electrically as well as mechanically.

Mechanical loading of solder joints occur during service conditions and the joints may be subjected to a series of tensile or shearing forces. The solder joints comprise of a stack of thin metal film, multi layered structures which include the solder balls, under-bump metallizations (UBM), base metals such as the copper pads and also the intermetallic compounds (IMC) formed (as a result of reflow and ageing).

The stability and reliability of the joining is largely determined by the ability of the structure to withstand the thermomechanical stresses generated. In particular, crack initiation and propagation in solder joints dominates as the main cause of failure and therefore fracture toughness arises as an important in the design for reliability. The failure modes in the solder joints can be adhesive (interface failures between solder and metallization) or cohesive (failure through the solder joint) in nature [1, 2]. Bulk solders have been used for tensile test in dog bone configuration [3] in order to extract properties like yield strength, modulus from stress-strain curve, its creep behaviour as a function of tensile loading speeds, Arrhenius dependency and etc. However, the properties of bulk solder specimens may not be reflective of solder joints. Therefore, testing of joints would ensure that the effects of microstructural changes have been accounted for [4] and the development of interface crack would be closely related to the actual product [5].

In practice, there are two main ways [6, 7] to characterize interfacial fracture. Based on the conventional "material strength" based approach, interfacial strength can be defined as the maximum stress that an interface can withstand. Expressing the strength in terms of unit stress, it could be measured by techniques such as tensile test or shear test.

The lap shear test is a rather straightforward method and is possibly the easiest to prepare and easy to test as no complicated fixtures or special equipment are required. While there are variations in the configuration of the specimen preparation and testing methodology [4, 8-11], the fundamental concepts are the same. Another popular technique widely used is ball shear testing [12-14], which can also be used to determine the bond strength between the solder ball and the substrate.

Tensile tests of solder joints are also adopted to study the interfacial failures in the microstructures and the effects of reflow, aging and surface finishes [15-18]. Solder joint in the form of arrays [17] or designed geometry [15, 16] could be employed to measure adhesion, such techniques are quick and easy to perform and give values of bond strength for comparisons.

The other approach is the "fracture mechanics" analysis. Interfacial fracture toughness is measured by an interface's resistance to decohesion and is of critical interest to be able to quantify and predict interface reliability. Interfacial fracture toughness characterizes when the existing crack will advance. The crack tip deformation dissipates energy and this is a primary contributor to interfacial fracture toughness.

The energy based failure criterion such as critical energy release rate, G_c is based on Linear Elastic Fracture Mechanics (LEFM) which is applicable only in cases where localized, small scale yielding at crack tip is observed. The plastic zone size is limited to a small area in front of the interface crack. Therefore, test specimens have to provide stable and controlled crack propagation for an accurate assessment of interface fracture energy [19]. Highly dependent on mode mixity, the stress field surrounding a crack tip can be characterized as mode-I (normal) or mode-II (shear) depending on the type of load applied to the crack and the stress fields surrounding the crack tip.

For the fracture mechanics approach, sandwich test specimens have become extremely popular. These sandwich

978-1-4244-2118-3/08/$25.00 ©2008 IEEE

structures exist in various forms such as four-point bend [20] , double cantilever beam (DCB) [21], and Brazil-nut specimens [22]. The theoretical basis for sandwich specimens to measure the interfacial fracture toughness was developed by Suo and Hutchinson [23].

While four point bend specimens have been widely used to characterized multi-layered thin film stacks in the semiconductor industry, when the interface joint is strong, the crack tends to propagate into the adherend(s) if they are brittle [24] and hence the interface energy data cannot be used. On the other hand, Brazil nut test specimens are able to provide mix mode G_c values but require complex mathematical calculations coupled with finite element analysis to obtain the necessary critical energy release rate [5, 20, 22].

The DCB technique which allows the characterization of mode I fracture toughness is an extremely useful and easy to implement technique as compared to the other two variants [19, 21, 24] and is employed in this paper as a fracture mechanics based assessment scheme to study the interface reliability of solder joints as a function of processing conditions. The DCB test can also be applied to the fracture toughness of monolithic solder alloys and intermetallic compounds. Such work will be reported in future publication.

2.0 Experimental Procedures

The DCB specimens were fabricated from 99.9wt% copper blocks and the dimensions of one of the mating surface is shown in Figure 1. Pin holes were machined at one end of the DCB adherends from which tensile loads could be applied to the specimens.

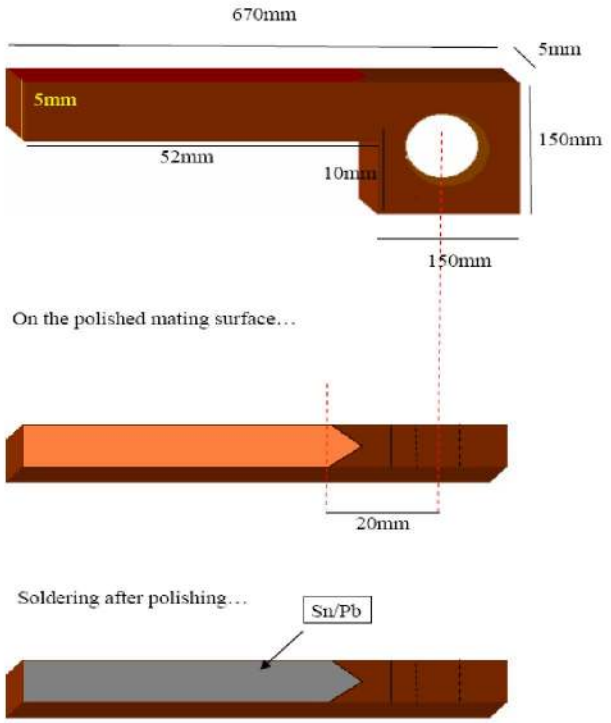

Figure 1: The DCB sandwich test specimen

The mating surfaces were mechanically polished using 800 grit followed by 1000 grit and 1200/2400 silica sandpaper. The aim was to create a smooth finish for reproducible testing results. This was followed by cleaning in acetone solution to remove dirt or debris from the surfaces. Cleaning the surface of the mating surfaces also serves the purpose of removing any copper oxide layer present. This is due in part to the high affinity copper has to oxygen and results in the oxidation of copper which reduces the adhesion strength of the die attach to the copper surface.

An additional copper etching recipe was introduced to delay oxide formation on the newly polished copper plate before soldering. The etching was done so that copper oxide will not pose an obstacle to a good soldering on the mating surface. Acetic acid (pure to no more than 4 vol% of water dilution) at 35°C for 5 – 10 minutes can effectively remove the surface oxide. Thermal tape is then applied to induce the initial crack (seen from the mating surface in the form of an arrow). This tapered surface, after solder joining, serves the purpose of initiating a sharp natural crack to the full sample width without using the conventional fatigue crack initiation method.

Following this, the cantilever beam samples were coated with Cu/Au layers by sputtering process. The sputtering conditions for each layer are shown in Table 1 below.

Table 1: The sputtering conditions for each layer on the etched copper substrate

	Cu	Au
Thickness	1.5µm	50nm
Time Taken	45min	0.5min
Power (DC)	250W	300W

Two DCB adherends with the mating surface facing each other were bonded together by a solder joint thickness of 1mm using eutectic 63Sn/37Pb solder wires and Alpha WS-709 water soluble solder paste. The wires/paste were applied directly to the surfaces of the adherends where 288mm of solder wire was the approximate equivalent of 1g of solder paste. In order to obtain the sandwiched solder joint structures, the specimen was sent for reflow using the profile illustrated in Figure 2 below.

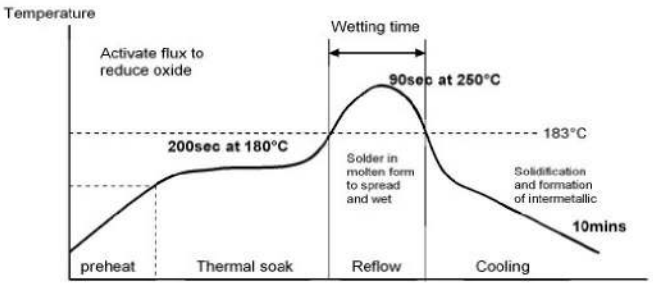

Figure 2: The reflow profile for DCB specimens

In this work, a total of 3 different cases of reflow profiles will be studied. See Table 2. For case 1, the DCB specimens under went a normal reflow of 90s at 250°C. Both solder wires as well as solder paste sandwiched specimens were prepared

for this case and it acts as a control case. DCB sandwiched specimens in case 2 and 3 also undergo the normal reflow like case 1 but had enhanced reflow condition of 10mins at 250°C and aging for 100hrs at 150 °C.

Table 2: Varied reflow conditions of DCB samples prepared

Condition	Form of applied solder	Reflow profile
Case 1	Solder wires/solder paste	Normal reflow: 90s at 250°C
Case 2	Solder paste	Normal reflow: 90s + enhanced reflow 10mins at 250°C
Case 3	Solder paste	Normal reflow: 90s + aging for 100hrs at 150°C

The specimens were loaded in tensile on an Instron Universal Tensile Tester 5567 as shown in Figure 3. For each specimen, increasing tensile loads were applied until the critical load P_c at the onset of failure of the solder joint was recorded.

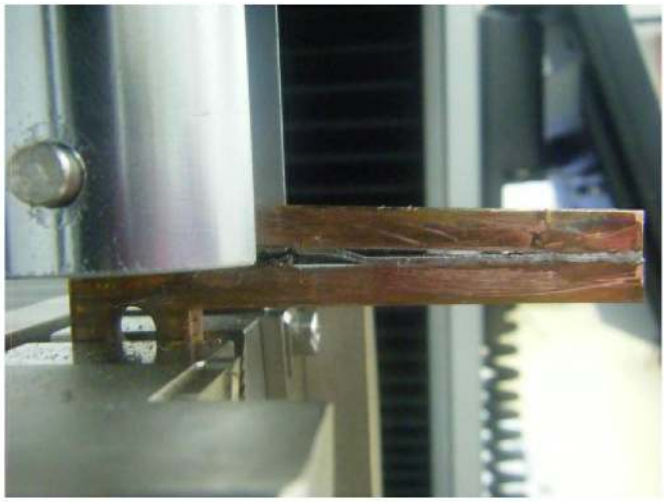

Figure 3: A DCB sample loaded by the Instron tester 5567

A sample size of three specimens was performed for each of the cases and the peak load was recorded. The tensile test was performed at room ambient conditions with a constant crosshead speed of 1mm/min until complete fracture of the specimen was attained. A JEOL 6360 SEM was subsequently used for surface and cross sectional analysis of the specimens. Energy dispersive X-ray (EDX) was also performed to analyze the chemical composition of the microstructure and also to determine and understand the crack path propagation in the DCB solder joint specimens.

3 Results

3.1 Load-displacement Records of the DCB Solder Test

The tension force measured shows a load versus displacement curve. Typical load versus displacement plots for the DCB solder joint specimens A1-A12 are shown in Figure 4. An interesting feature of this work is the presence of a load plateau before the subsequent increase to P_c. This allows a steady state crack propagation to develop before the joint reaches the peak load and fail.

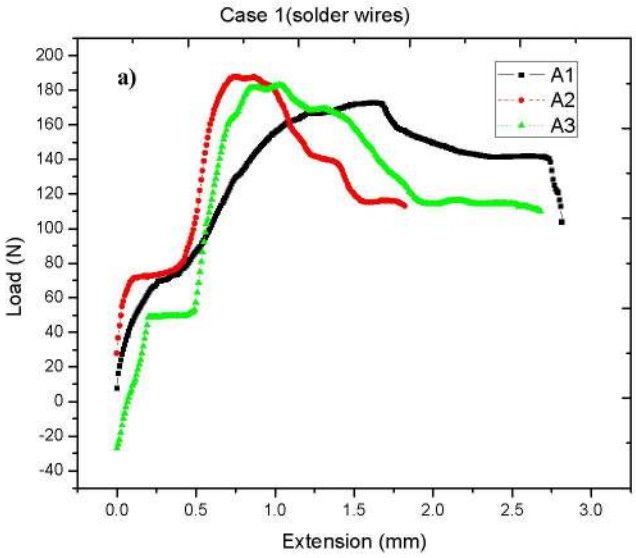

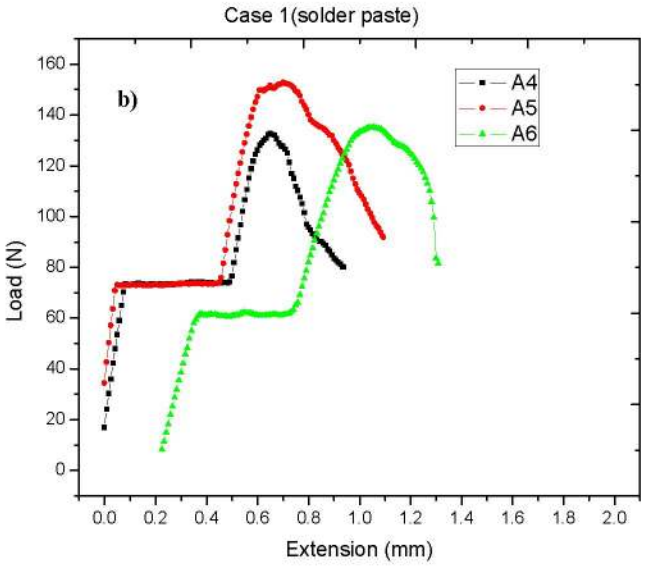

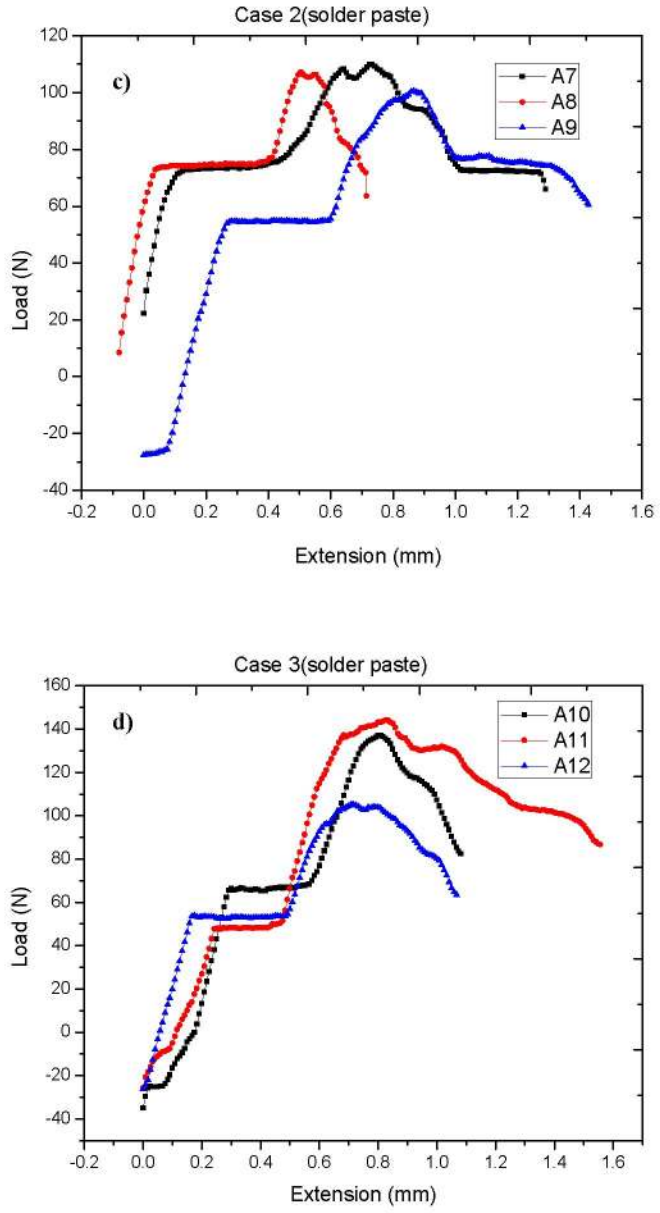

Figure 4: Typical load-displacement curves for (a) Sn/Pb wires under normal reflow of 90s at 250°C, (b) Sn/Pb paste under normal reflow of 90s at 250°C, (c) under normal reflow of 90s at 250°C plus enhanced reflow for 10mins at 250°C, (d) under normal reflow of 90s at 250°C plus ageing for 100hrs at 150°C.

It can be observed that for case 1, under normal reflow of 90s at 250°C, the maximum tensile load sustained by the solder wires fabricated joints is much higher as compared to solder pastes prepared sandwiched joints. In addition, the breaking load of the solder joints prepared by the paste method also dropped with the increase in enhanced reflow for 10mins at 250°C and ageing of the joints at 150°C for 100hrs. The solder joint degradation for the enhanced reflow (Case 2) is more severe than continuous ageing (Case 3).

3.2 Interface Fracture Toughness of solder joint specimens

The peak loads obtained were used in fracture mechanics analysis to quantify the fracture energy. According to the classical beam theory, the measure of material resistance to decohesion can be quantified by the energy release rate at the onset of stable crack growth, G. For a double cantilever beam under mode I loading is derived to be

$$G = \frac{12P^2a^2}{b^2h^3E} \quad (1)$$

where b is the width and h is the thickness of a single beam, a is the crack length, P is the load, and E is the modulus of the copper adherend.

From the graphs, it was observed that the peak loads for three different samples in one set of cases may vary in magnitude. The scatter in recorded data may be attributed to the differences in the crack length for each prepared specimen. However, after taking into consideration the differences in crack length, the critical energy release rate (G_c) of the samples was calculated using equation 1. The distribution of G_c data values for the samples may be attributed to the slight variation of solder thickness for each joint specimen. Therefore an average of the 3 individual G_c values were taken.

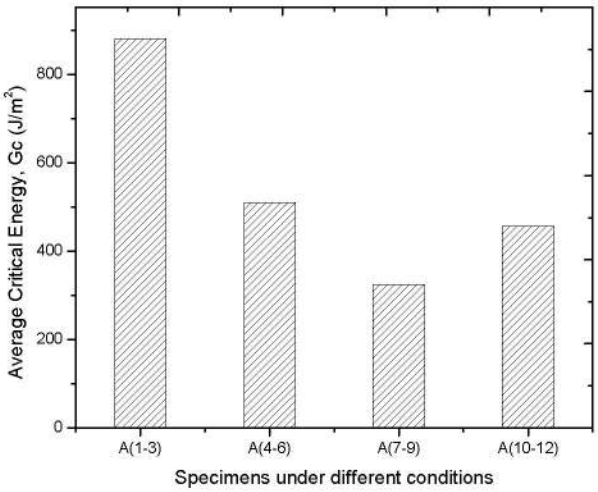

Figure 5: Average critical energy release rate, G_c for the DCB sandwich specimens under different process conditions prescribed by Table 2.

As energy release rate, G_c is proportional to the square of the critical load, P_c (see equation 1) the parameter of importance is the P_c which is obtained from the load as a function of displacement curves shown in Figure 4. The higher the magnitude of G_c, the greater the strength of the solder joint. G_c obtained for solder wires in case 1 is the highest, followed by the solder paste under normal reflow conditions. As per the trend in section 3.1, when enhanced reflow was performed, the G_c decreased by a substantial amount. In comparison, high temperature ageing at 150°C does degrade the joint and resulted in a modest decrease in G_c.

3.3 Fracture Analysis of Microstructures

After the fracture test, the broken specimens were characterized using a scanning electron microscope (SEM) equipped with energy dispersive spectroscopy (EDS) for microstructure and compositional analysis. The failure paths of the sandwich solder joints are usually along the interface between the copper adherend and solder joint See Figure 6.

There were several cases of necking in the bulk eutectic 63Sn/37Pb solder. It was also possible for solder to debond from the other interface as a result of tearing which indicate a possibility of ductile deformation before fracture. However, as the crack path propagation is generally confined to the copper/solder interface, it shows that the adhesive strength of the interfacial metallic compound formed is weaker as compared to the cohesive strength of the bulk solder which alluded to the eventual crack path growth.

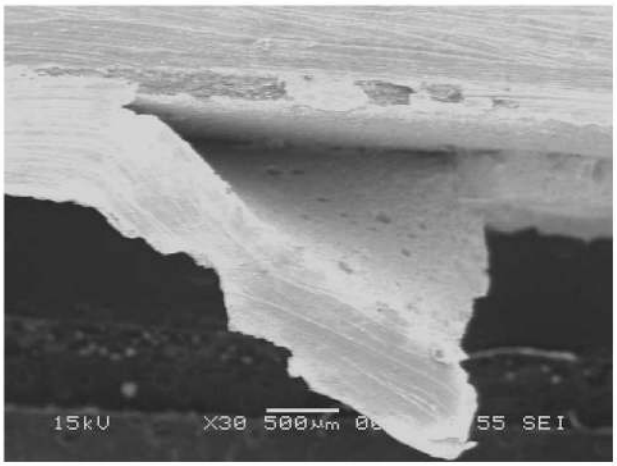

Figure 6: Micrograph of specimen A10 (100hrs of ageing at 150 °C).

Further investigations into the failure paths were conducted. Figure 7 shows a selection of SEM micrographs, each from one of the cases described in Table 2.

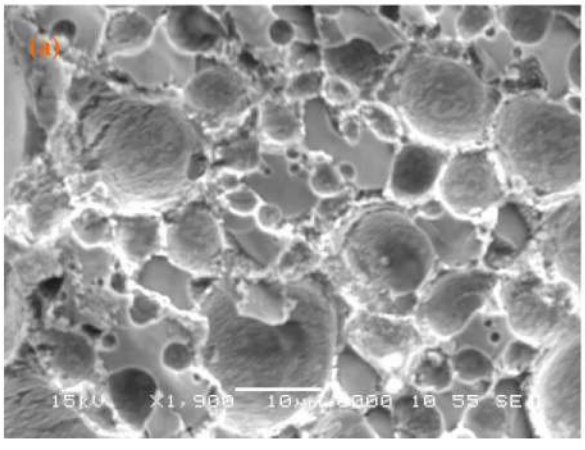

Specimen A2: Sn/Pb wires under normal reflow of 90s at 250°C

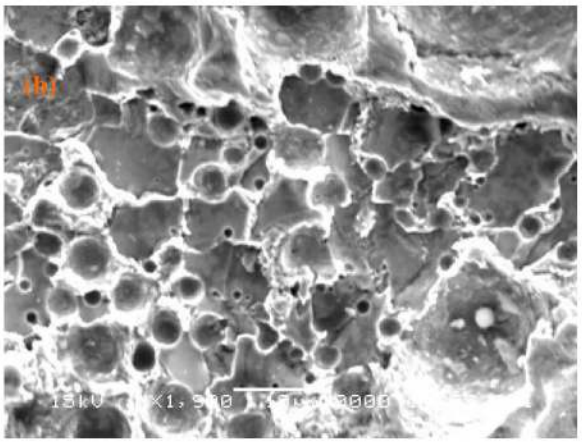

Specimen A4: Sn/Pb paste under normal reflow of 90s at 250°C

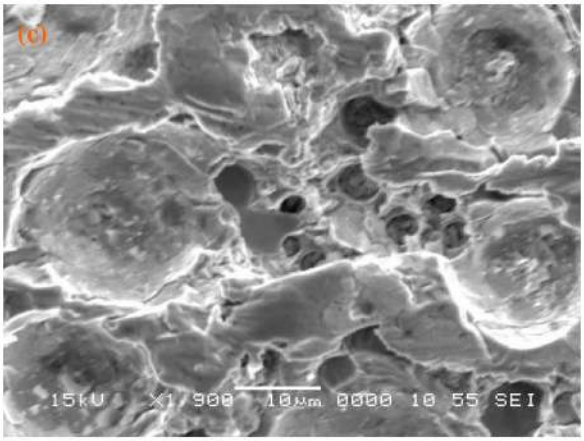

Specimen A9: Sn/Pb paste under normal reflow of 90s at 250°C plus enhanced reflow for 10mins at 250°C

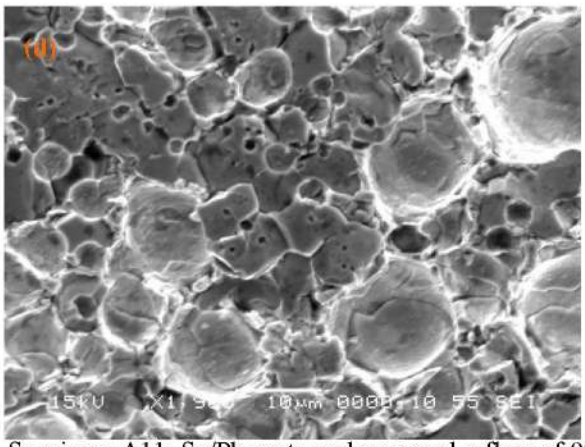

Specimen A11: Sn/Pb paste under normal reflow of 90s at 250°C plus ageing for 100hrs at 150°C.

Figure 7(a-d): Fracture surfaces of the soldered specimens from all 3 cases.

The fracture surfaces in Figure 7 shows that despite the different process conditions that the joint had been subjected to, their failure modes were quite similar. The separation at the interface was between the IMCs and the bulk solder. Dimples and voids were also produced in the process of IMC

delaminating from the bulk solder. This is the case where a hard particle (IMCs) separates from the soft matrix (solder). Figure 8 shows the mating surface of fracture specimen A4. EDX analysis performed on the fractured interface confirmed the findings that failure was normally between the Cu_6Sn_5 IMCs and the solder. Typically the hard IMC also experiences brittle cleavage failure resulting in relatively flat and abruptly truncated surfaces.

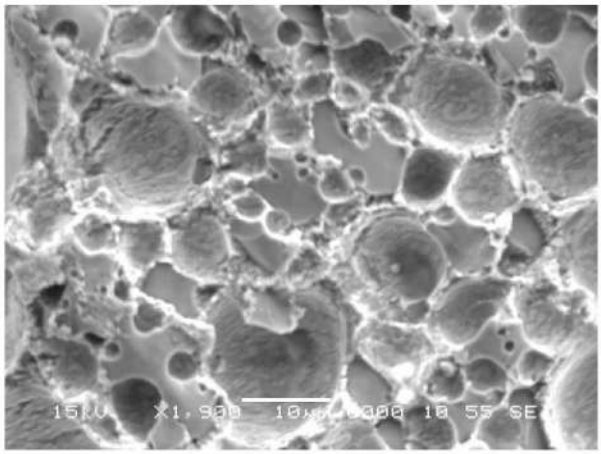

Figure 8: The mating surface of specimen A4

For case 1:

The SEM and EDX analysis on the top and cross sectio fracture surface showed the atomic ratio of Cu to Sn in t IMC for Specimen A2, the ratio was about 6:5 whi corresponds to the Cu_6Sn_5 IMC. No Cu_3Sn IMC was detect in this case.

As compared to Specimen A1, A2 and A3, these solc paste samples were pre-soldered onto the mating surfa before reflow. Interfacial reactions have spontaneou occurred the moment solder touches the mating surface.

However for both batches, the formation of Cu_6Sn_5 lay was not thick and significant enough to have resulted decrease in fracture toughness so that fracture may occur the Cu_6Sn_5 layer. Instead, the solder joint failed through the interface of Cu_6Sn_5/ solder and is a mixed fractured path. However, presence of voids in solder paste specimens as a result of residual flux contributes to the reduction in strength of the solder joints. This can also be seen in the general grouping of data of solder wires versus solder paste specimens i.e. A1-A3 and A4 – A12 respectively.

For case 2:

The soldered joint failed through trace areas of Cu_6Sn_5 IMC and the majority of the fracture path took place at the solder/IMC interface. This suggests that case 2 was a mixed fracture as well. The increased in exposure time at high reflow temperatures have caused the intermetallic layer at the interfacial boundary to grow in thickness resulting in decreases in fracture toughness so that fracture may occur at this intermetallic layer. An obvious distinction between specimens in case 2 as compared to those in case 1 and 3 is that the dimples formed by the fracture path are much shallower and larger. This indicates a reduction in ductility and increase in brittleness at the microscopic scale. The critical energy release rate is also therefore the lowest among all the samples.

For case 3:

The soldered joint failed through mostly at the solder/Cu_6Sn_5 mixed phase layer. Therefore it can be concluded that failure paths for thermally aged specimens in this work is similar to the as soldered specimens when subjected to tensile testing. An interesting feature found was that Cu_3Sn could be observed. The resulting analysis reflected the atomic ratio of Cu to Sn in the IMC for Specimen A11, the ratio was about 3:1 which corresponds to the Cu_3Sn IMC. Low detection level of Cu_3Sn is most likely due to short solid state aging time for the Cu_3Sn to become prominently visible. For this solid state reaction, aging time can amount up to 1000hrs but due to time constraint, experiment was set only at 100hrs.

The salient features of this microstructure and the corresponding EDX analysis is shown in Figure 9.

Element	(keV)	mass%	Error%	At%	Compound		mass%	Cation	K
O		20.69							
Ca K	3.690	1.30	0.28	3.11	CaO	1.82	0.60	2.0920	
Cu K	8.040	47.96	1.67	72.55	CuO	60.03	14.00	63.5112	
Sn L	3.442	30.05	0.58	24.34	SnO2	38.15	4.70	34.3968	
Total		100.00		100.00		100.00	19.30		

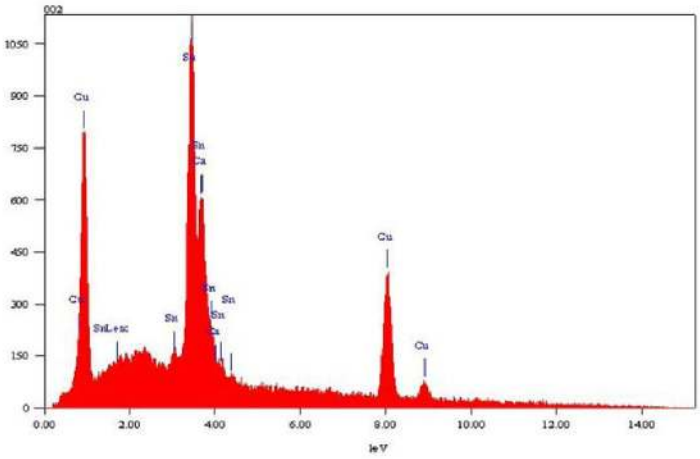

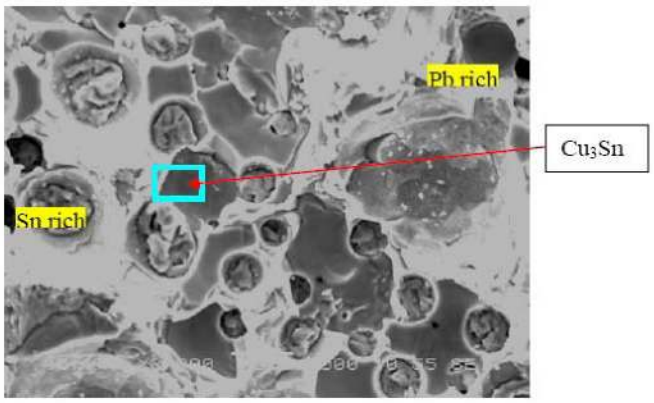

Figure 9: EDX analysis spectrum of specimen A11 showing the presence of Cu_3Sn

A Pb-rich zone is shown to form in the solder, adjacent to the Cu_3Sn, when the intermetallics are grown in a solidified solder joint by thermal aging. The Sn is depleted locally by the

reaction with copper that forms the Cu_3Sn. This zone is a discrete layer for moderate amounts of solid state thermal aging, but it can become discontinuous after extensive aging. In either case, this zone is also a potential weak link in the solder joint.

Voids were also found on the fractured major Cu_6Sn_5 surface. This is an indication that the voided IMC layer is an easy path for cracks to go through, resulting in brittle fracture. The situation of the Sn/Pb solder joint might be worse because the Cu_6Sn_5 layer, where the voids are located, is very thin so that after the formation of voids, it becomes discontinuous. Cracks can easily propagate through this layer, leading to failure.

4.0 Discussions - Fracture Crack Path Mechanism

In order for the proper formation of metallurgical bond during solder, the presence of IMCs is almost always necessary. However, the excessive growth of intermetallics affects the reliability of the solder joint. The DCB sandwich eutectic Sn63/Pb37 solder joint consist of 4 main constituents, namely the solder, the IMCs, Cu_6Sn_5 and Cu_3Sn and the copper adherends. The material properties of these four constituents are given in [25]. Cu_6Sn_5 is the hardest followed by Cu_3Sn then copper and finally solder. The high hardness of also makes it extremely brittle and it is the site of the maximum stress concentration in a solder joint, particularly the protruding region of Cu_6Sn_5. A schematic of a typical solder joint is shown in Figure 10.

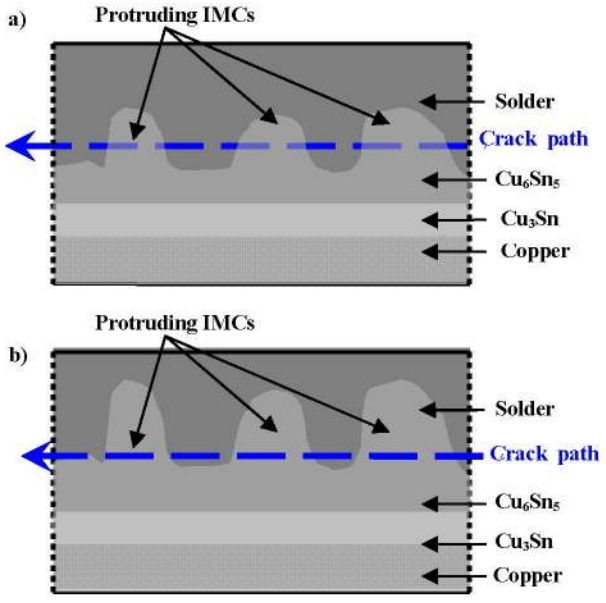

Figure 10: A schematic segment of the solder joint constituents under (a) as soldered conditions and (b) extended reflow or prolonged ageing conditions

The arrow shaped pre-crack (See Figure 1) acts as a point of stress concentration which allows the crack to grow along a path parallel to the interface between the Cu_3Sn and solder interface. The crack path propagates and upon reaching the brittle Cu_6Sn_5 protruding grains, breaks them and continues its propagation into the solder creating the dimple like morphology observed. All three cases in this study had such a microstructure which also indicates a mixed mode failure of fracture within the Cu_6Sn_5 IMC and the Cu_6Sn_5 /solder interface.

Under extended reflow and isothermal high temperature ageing conditions as prescribed by cases 2 and 3 respectively, the coarsening of the microstructure of the solder joint is expected. In addition, the IMC layer thickness is also expected to increase as illustrated in Figure 10b). The increase in thickness of this brittle layer is expected to decrease the tensile strength and hence lower the G_c of the solder joint. While the crack path mechanism is similar, it could be observed that the dimple like morphology on the as soldered specimens in case 1 become shallower and a transition to a more cleavage like fractography as seen in cases 2 and 3.

A cross section of specimen A5 in Figure 11 clearly illustrates the proposed failure mechanism. In Figure 11a), the Cu_6Sn_5 intermetallics could be clearly ascertained due to the scallop formations as a result of interfacial reaction between the Cu and solder. Figure 11b) taken from a cross sectional view of the fracture interface shows the undulating nature of the failure paths that runs between the Cu_6Sn_5 IMC and the solder/Cu_6Sn_5 which verifies the proposed mechanism.

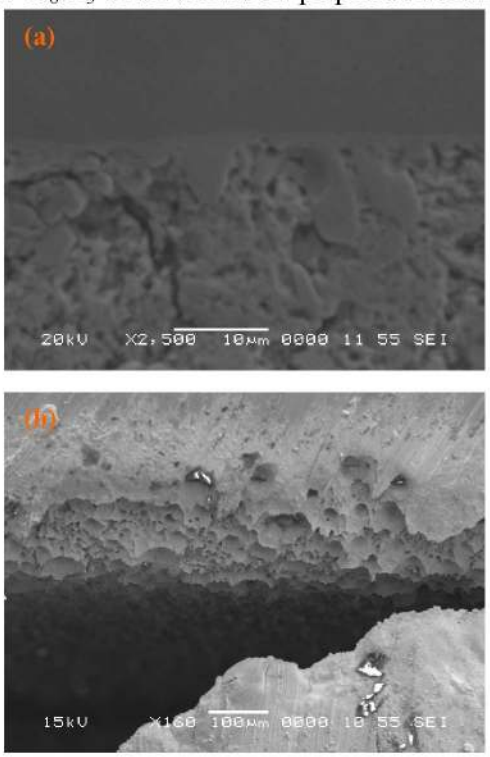

Figure 11: Specimen A5 in cross-sectional view (a) of Cu_6Sn_5 scallop formations and (b) dimple morphology due to separation of soft solder from hard intermetallics Cu_6Sn_5.

5 Conclusions

A fracture toughness assessment methodology for solder joint fracture toughness was developed in this work. Studies were performed to study the effects of processing parameters such as extended reflow and isothermal annealing that may degrade the fracture toughness of solder joints. Results offered were conclusive and provided good experimental repeatability. By adopting a fracture mechanics approach, the critical energy release rate, G_c could be quantified explicitly. Fracture crack path mechanism was observed in all three cases

to be generally confined to the solder/IMC interface which was the weakest link in the DCB sandwich configuration.

Acknowledgments

The authors would like to thank Economic Development Board (EDB) of Singapore for funding of this project under Innovation Development Scheme (IDS).

References

1. J. Abdul, Y. Wang, N. Guo, A. U. Rehman, and K. C. Chan, "Ultrasonic evaluation of the silicon/copper interfaces in IC packaging," IEEE Transactions on Electronics Packaging Manufacturing, vol. 26, pp. 221-227, 2003.
2. H. L. J. Pang, X. R. Zhang, C. H. Lim, X. Q. Shi, and Z. P. Wang, "Interfacial fracture toughness test methododology for flip chip underfill encapsulant," 52th ECTC Conference Proc., 2002, pp. 1640-1644.
3. J. H. L. Pang, B. S. Xiong, C. C. Neo, X. R. Zhang, and T. H. Low, "Bulk solder and solder joint properties for lead free 95.5Sn-3.8Ag-0.7Cu solder alloy," 53th ECTC Conference Proc., 2003, pp. 673-679.
4. R. Darveaux and C. Reichman, "Mechanical properties of lead-free solders," 57th ECTC Conference Proc., 2007, pp. 695-706.
5. S. Loo, X. Zhang, H. S. Ng, T. Y. Tee, and S. G. Mhaisalkar, "Impact of thermal, moisture, and mechanical loading conditions on interfacial fracture toughness of adhesively bonded joints," Journal of Electronic Materials, vol. 36, pp. 110-116, 2007.
6. B. Lauke and T. Schueller, "Essential work of interfacial fracture: A method to characterize adhesion at polymer-polymer interfaces," International Journal of Adhesion and Adhesives, vol. 21, pp. 55-58, 2001.
7. Y. Qizhou, Q. Jianmin, W. Jiali, and C. P. Wong, "Characterization of underfill/substrate interfacial toughness enhancement by silane additives," IEEE Transactions on Electronics Packaging Manufacturing, vol. 26, pp. 264-267,1999.
8. W. H. Moy and Y. L. Shen, "On the failure path in shear-tested solder joints," Microelectronics Reliability, vol. 47, pp. 1300-1305, 2007.
9. Y. L. Shen, N. Chawla, E. S. Ege, and X. Deng, "Deformation analysis of lap-shear testing of solder joints," Acta Materialia, vol. 53, pp. 2633-2642, 2005.
10. B. J. Van de Wal, G. Kendall, B. Sammakia, C. Sahay, and J. Constable, "Acoustic emission analysis for fatigue prediction of lap solder joints in mode two shear," International Journal of Damage Mechanics, vol. 10, pp. 256-276, 2001.
11. R. Darveaux, "Shear deformation of lead free solder joints," 55th ECTC Conference Proc., 2005, pp. 882-893.
12. J. Y. H. Chia, B. Cotterell, and C. Tai Chong, "The mechanics of the solder ball shear test and the effect of shear rate," Materials Science & Engineering A (Structural Materials: Properties, Microstructure and Processing), vol. 417, pp. 259-274, 2006.
13. J. W. Kim, J. Joo, D. J. Quesnel, and S. B. Jung, "Correlation between displacement rate and shear force in shear test of Sn-Pb and lead free solder joints," Materials Science and Technology, vol. 21, pp. 373-380, 2005.
14. S. W. R. Lee and H. Xingjia, "Analysis on solder ball shear testing conditions with a simple computational model," Soldering & Surface Mount Technology, vol. 14, pp. 45-48, 2002.
15. A. Kumar, Z. Chen, S. Mhaisalkar, C. C. Wong, P. S. Teo, and V. Kripesh "Effect of Ni-P Thickness on Solid-State Interfacial Reactions between Sn-3.5Ag Solder and Electroless Ni-P Metallization on Cu Substrate", Thin Solid Films, Vol. 504 (1-2), pp. 410-415, 2006
16. Z. Chen, M. He, A. Kumar, and G. J. Qi, "Effect of interfacial reaction on the tensile strength of Sn-3.5Ag/Ni-P and Sn-37Pb/Ni-P solder joints," Journal of Electronic Materials, vol. 36, pp. 17-25, 2007.
17. R. Darveaux, C. Reichman, and N. Islam, "Interface failure in lead free solder joints," 56th ECTC Conference Proc., 2006, pp. 906-917.
18. K. H. Prakash and T. Sritharan, "Tensile fracture of tin-lead solder joints in copper," Materials Science and Engineering A, vol. 379, pp. 277-285, 2004.
19. T. K. Lee, "Interfacial adhesion studies using double cantilever beam method and shear testing," 9th EPTC Conference Proc., Singapore, 2007, pp. 571-575.
20. A. A. Volinsky, N. R. Moody, and W. W. Gerberich, "Interfacial toughness measurements for thin films on substrates," Acta Materialia, vol. 50, pp. 441-466, 2002.
21. F. Aviles and L. A. Carlsson, "Analysis of the sandwich DCB specimen for debond characterization," Engineering Fracture Mechanics, vol. 75, pp. 153-168, 2008.
22. A. Kuhl and Q. Jianmin, "A technique to measure interfacial toughness over a range of phase angles," Transactions of the ASME. Journal of Electronic Packaging, vol. 122, pp. 147-151, 2000.
23. Z. Suo and J. W. Hutchinson, "Sandwich test specimens for measuring interface crack toughness," Mater. Sci. Eng., vol. A107, 1989, pp. 135-143.
24. X. Fan, Z. Jiang, and A. Chandra, "Package structural integrity analysis considering moisture," 58th ECTC Conference Proc., 2008, pp. 1054-1066.
25. H.-T. Lee, M.-H. Chen, H.-M. Jao, and T.-L. Liao, "Influence of interfacial intermetallic compound on fracture behavior of solder joints," Materials Science and Engineering A, vol. 358, pp. 134-141, 2003.